

Measurement of Inclusive ω and η' Production in Hadronic Z Decays

M. Acciarri, O. Adriani, M. Aguilar-Benitez, S. Ahlen, B. Alpat, J. Alcaraz, G. Alemanni, J. Allaby, A. Aloisio, G. Alverson, et al.

► To cite this version:

M. Acciarri, O. Adriani, M. Aguilar-Benitez, S. Ahlen, B. Alpat, et al.. Measurement of Inclusive ω and η' Production in Hadronic Z Decays. Physics Letters B, Elsevier, 1997, 393, pp.465-476. in2p3-00014307

HAL Id: in2p3-00014307

<http://hal.in2p3.fr/in2p3-00014307>

Submitted on 24 Nov 1998

HAL is a multi-disciplinary open access archive for the deposit and dissemination of scientific research documents, whether they are published or not. The documents may come from teaching and research institutions in France or abroad, or from public or private research centers.

L'archive ouverte pluridisciplinaire **HAL**, est destinée au dépôt et à la diffusion de documents scientifiques de niveau recherche, publiés ou non, émanant des établissements d'enseignement et de recherche français ou étrangers, des laboratoires publics ou privés.

Measurement of Inclusive ω and η' Production in Hadronic Z Decays

The L3 Collaboration

Abstract

We present a study of the inclusive ω and η' production based on 3.1 million hadronic Z decays recorded with the L3 detector at LEP during 1991–1994. The production rates per hadronic Z decay have been measured to be 1.17 ± 0.17 ω mesons and 0.25 ± 0.04 η' mesons. The production rates and the differential cross sections have been compared with predictions of the JETSET and the HERWIG Monte Carlo models. We have observed that the differential cross sections can be described by an analytical quantum chromodynamics calculation.

(To be submitted to *Physics Letters B*)

Introduction

Experimental studies of spectra and composition of particles in e^+e^- annihilation are important for understanding the fragmentation of quarks and gluons into hadrons. Fragmentation is not perturbatively calculable and at present it can only be described by phenomenological models. Many particle species have been extensively studied in e^+e^- annihilation at lower energies [1], and recently, a large amount of information on identified hadron species has become available at LEP [2]. However, few e^+e^- experiments [3–6] have measured the production of ω and η' mesons. The η' production rate is of interest since it provides information on the transformation of the SU(3) states (η_8, η_1) into the observed states (η, η'). Also, uncertainties on the η' production rate can have an effect on other measurements, for example, the Bose-Einstein correlation of charged pions [7] and particle multiplicities. Furthermore, the measured η' production rate [4] differs significantly from the prediction of JETSET 7.3 [8].

In this paper, we report on a measurement of inclusive production of ω and η' mesons in hadronic Z decays using the L3 detector at LEP. The ω is identified via its decay channel $\omega \rightarrow \pi^+\pi^-\pi^0$, while the η' is reconstructed via its decay channels $\eta' \rightarrow \pi^+\pi^-\eta$ and $\eta' \rightarrow \rho^0\gamma$. The π^0 and η mesons are detected through their two-photon decay channels as narrow peaks in the $\gamma\gamma$ invariant mass distribution, while the ρ^0 meson is reconstructed via its decay channel $\rho^0 \rightarrow \pi^+\pi^-$. The production rates and differential cross sections as a function of the scaled momentum $x_p = p/p_{beam}$ are measured and compared with the predictions of two Monte Carlo generators. A parton cascade based on perturbative QCD calculations is used in both generators, while the non-perturbative hadronization phase is described by either string (JETSET 7.3) or cluster fragmentation (HERWIG 5.4 [9]) models.

We also measure the dependence of the differential cross section on the variable $\xi = \ln(1/x_p)$. Under the local parton-hadron duality assumption [10, 11], the measured cross section can be compared with predictions of the modified leading log approximation (MLLA) of QCD [10].

The L3 Detector

The L3 detector is described in detail in Ref. [12]. It consists of a central tracking chamber, a high resolution electromagnetic calorimeter composed of bismuth germanium oxide (BGO) crystals, a ring of plastic scintillation counters, an uranium and brass hadron calorimeter with proportional wire chamber readout, and an accurate muon chamber system. These detectors are installed in a 12 m diameter magnet which provides uniform field of 0.5 T along the beam direction.

The central tracking chamber (TEC) is a time expansion chamber with high spatial resolution in the plane normal to the beam. A Z-chamber, mounted just outside the TEC, supplements the r/ϕ measurements with z-coordinates. Starting from 1994, tracks are also measured by a silicon micro-vertex detector consisting of two layers of silicon with double-sided readout [13].

The material preceding the barrel part of the electromagnetic detector amounts to less than 10% of a radiation length. In this region the energy resolution is 5% for photons and electrons of energy around 100 MeV, and is less than 2% for energies above 1 GeV. The angular resolution of electromagnetic clusters is better than 0.5° for energies above 1 GeV.

For this analysis, we use the data collected in the following polar angle ranges: for the central tracking chamber $40^\circ < \theta < 140^\circ$; for the electromagnetic calorimeter $11^\circ < \theta < 169^\circ$; and for the hadron calorimeter $5^\circ < \theta < 175^\circ$.

Data Selection

For this analysis, we use events collected at center of mass energies near the Z mass ($88.4 \leq \sqrt{s} \leq 93.7$ GeV) during the 1991–1994 LEP running periods. The data correspond to an integrated luminosity of 112 pb^{-1} .

The selection of events of the type $e^+e^- \rightarrow \text{hadrons}$ is based on tracking information as well as on the energy measured in the electromagnetic detector and in the hadron calorimeter. Events are accepted if they have high multiplicity and high and well balanced visible energy [14]. In total, 3.1 million events pass the selection cuts.

About 2.3 million hadronic events generated by the Monte Carlo program JETSET 7.3 [8] are used in the analysis. In addition, 430,000 events generated using HERWIG 5.4 [9] are used to check for systematic effects due to different fragmentation models. The values for the QCD scale and the fragmentation parameters in both Monte Carlo programs were determined from fits to our previous measurements [15]. The generated events are passed through the L3 detector simulation [16], which implements a detailed description of the detector and takes into account the effects of energy loss, multiple scattering, interactions and decays in the detector materials and the beam pipe. These events are processed with the same reconstruction and analysis programs as used for the experimental data.

Applying the same selection of hadronic Z decays to the simulated events as for the data, we find that more than 99% of the hadronic decays from the Z are accepted. The contamination from e^+e^- and $\tau^+\tau^-$ final states and from hadronic production via two-photon processes is estimated to be less than 0.2% and is ignored in the following analysis.

Photon Selection

Photon candidates are recognized as isolated clusters in the electromagnetic calorimeter. The photon energy is calculated from the energy of the cluster by applying a position-dependent correction. Assuming that the photon originates at the e^+e^- interaction point, its direction is determined from the center of gravity of the shower.

The photons used in this analysis are required to be in the barrel region, $|\cos\theta_\gamma| < 0.74$. Their energy has to be greater than 100 MeV. The lateral shower shape of the photon candidate has to be consistent with that of an electromagnetic shower, as determined by an artificial neural network [17] trained on a sample of Monte Carlo data. To further reduce the background from hadrons, the photon candidate must be separated by at least 50 mrad from any charged particle. The selection efficiency for inclusive photons in hadronic Z events is about 30% with a purity of about 70%.

Track Selection

To have good resolution in the invariant mass, we apply relatively tight selection cuts to charged tracks. Charged tracks have to be well measured in the central tracking chamber as well as the Z-chamber, with a momentum transverse to the beam axis of more than 100 MeV. Their distance of closest approach to the primary e^+e^- vertex in the $R\phi$ plane must be smaller than 2 mm. In addition, we exclude tracks passing through low resolution regions adjacent to the anode and cathode planes.

Extraction of the ω signal

The ω meson is measured in the decay channel $\omega \rightarrow \pi^+\pi^-\pi^0$. In a first step we reconstruct the π^0 through its two-photon decay channel. In order to reduce the combinatorial background, the $\gamma\gamma$ invariant mass spectrum is determined from pairs of photons produced in the same hemisphere defined with respect to the event thrust axis. For the analysis, only π^0 candidates with a reconstructed mass within ± 24 MeV ($\pm 3\sigma$) of the nominal mass of 135.0 MeV are used. The selected π^0 candidates are then combined with two charged tracks assumed to be pions. To reduce the large combinatorial background, we subtract the spectra for like-sign combinations ($\pi^\pm\pi^\pm\pi^0$) from those for unlike-sign combinations ($\pi^+\pi^-\pi^0$). As will be discussed below in the study of systematic errors, the final results are relatively insensitive to the procedures used to subtract the backgrounds.

The resulting ‘background-subtracted’ spectrum is shown in Fig. 1. An ω signal is clearly visible. There is also a small but clear η signal close to the kinematic threshold in the mass spectrum. We fit the spectrum with two Gaussian distributions for the ω and η signal respectively, plus a background function which is described by either a fifth-order polynomial or the following threshold function

$$BG(M) = (M - M_{th})^{p_1} \cdot \exp(p_2 M + p_3 M^2 + p_4 M^3),$$

where M_{th} is the threshold invariant mass of the decay products. The threshold function is found to yield better χ^2 and is therefore taken, while the polynomial is used in evaluating systematic uncertainties. The fit gives 25260 ± 1901 as the observed number of ω mesons. The mass is compatible with the PDG [18] value and the width is 28 MeV, in agreement with the expected detector resolution.

Extraction of the η' signal

The η' is measured in its two dominant decay channels, $\eta' \rightarrow \pi^+\pi^-\eta$ and $\eta' \rightarrow \rho^0\gamma$. For the decay channel $\eta' \rightarrow \pi^+\pi^-\eta$, the same procedure is applied as used for the extraction of the ω signal in the $\omega \rightarrow \pi^+\pi^-\pi^0$ channel, except that the η is used instead of the π^0 . The η is reconstructed through its two-photon decay channel. In order to reduce the combinatorial background related to π^0 decays, we exclude all photons entering into a two-photon combination with invariant mass inside the π^0 window. The invariant mass window for η candidates is set to be ± 50 MeV ($\pm 3\sigma$) around the nominal mass of 547.5 MeV. Because of limited phase space, $\pi\pi$ pairs from the η' decay tend to have low invariant mass. To further reduce the combinatorial background in combinations of $\pi\pi\eta$, we require the invariant mass of $\pi\pi$ pairs to be smaller than 0.4 GeV. The resulting ‘background-subtracted’ spectrum is shown in Fig. 2a. From the fit, in which a fourth-order polynomial is used for the background, we obtain 2989 ± 221 as the observed number of η' mesons. The mass is compatible with the PDG value and the width is 14 MeV, smaller than the measured width of the ω due to the lower energy available in the decay $\eta' \rightarrow \pi^+\pi^-\eta$.

For the decay channel $\eta' \rightarrow \rho^0\gamma$, we first reconstruct the ρ^0 in the channel $\rho^0 \rightarrow \pi^+\pi^-$. All combinations of two unlike-sign tracks with an invariant mass in a window of 150 MeV around the ρ^0 nominal mass are used. To reduce the combinatorial background in combinations of $\pi\pi\gamma$, a number of additional cuts are applied. The reconstructed direction of the ρ^0 and of the γ must both be inside a cone around the direction of the η' candidate, with a half opening angle varying linearly with the η' momentum p from 90° at $p=0$ GeV to 30° at $p=8$ GeV. The

cosine of the angle θ^* between the direction of the γ with respect to the η' direction in the η' rest frame is required to be $\cos(\theta^*) > -0.8$. As the η' is a spin 0 meson and ρ^0 and γ have spin 1, a helicity cut is applied. The cosine of the helicity angle θ^{**} between the γ and a pion in the in ρ^0 rest frame is required to be $|\cos(\theta^{**})| < 0.8$. In addition, it is required that the most energetic pion carries more than 20% of the energy of the $\rho^0\gamma$ system. Finally, we subtract the spectra for like-sign combinations ($\pi^\pm\pi^\pm\gamma$) from those for unlike-sign combinations ($\pi^+\pi^-\gamma$). The resulting ‘background-subtracted’ spectra are shown in Fig. 2b. The residual background is fitted with a threshold function and the signal with a Gaussian function. From the fits, a total of 10812 ± 910 η' are observed in $0.01 < x_p < 0.24$. The mass is compatible with the PDG value and the width is 19 MeV, consistent with the detector resolution.

Inclusive Production Rates

The selection efficiency for the ω and η' signal is determined from the Monte Carlo as the ratio of the ‘observed’ number of ω (or η') mesons to the number of generated ω (or η') mesons. In this way, our results are independent of the Monte Carlo simulation of the background and of the width of the signal. The resulting production rates determined from the ω and two η' decay channels are listed in Table 1 and compared with the Monte Carlo predictions. The rates are extrapolated to the full momentum range by means of the corresponding Monte Carlo predictions. Due to the different fragmentation schemes in the two models, there is a difference between JETSET and HERWIG in the isolation of photons. Therefore, the two Monte Carlo models give different selection efficiencies. As both models otherwise provide a reasonable description of the data [15], we take the average of the production rates determined by the two models as our result, assigning half of the differences to the systematic errors.

The first error in the last column of Table 1 is statistical, the second one is systematic. Besides the systematic error due to the choice of fragmentation models, other errors are obtained by varying the photon selection cuts, switching off the requirement on shower isolation from charged particles and changing the π^0 background suppression procedure. Errors due to the uncertainty in the detector efficiency are determined from a comparison of the π^0 and η rate in different geometrical regions of the detector. An additional small error due to the uncertainty of the TEC and the Z-chamber efficiency is taken into account. As mentioned above, two different functions have been used to describe the background shape in the fit. The function leading to the better χ^2 has been taken while the other was used in evaluating systematic uncertainties. For the decay channels $\omega \rightarrow \pi^+\pi^-\pi^0$ and $\eta' \rightarrow \pi^+\pi^-\eta$, we also use the π^0 and η sideband subtraction to estimate systematic effects in the background subtraction. In this case, $\gamma\gamma$ combinations from a π^0 (or η) sideband, combined with a $\pi^+\pi^-$ pair, are used for the background subtraction. Finally, the statistical error on the Monte Carlo events is included in the systematic errors. The size of these contributions is summarized in Table 2.

From the procedure described above, the ω rate per hadronic Z event is determined to be

$$N_\omega = 1.17 \pm 0.17.$$

In an independent analysis, the ω signal is studied via the decay channel $\omega \rightarrow \pi^0\gamma$, whose branching ratio is a factor of 10 smaller than that of the decay channel $\omega \rightarrow \pi^+\pi^-\pi^0$. The invariant mass spectrum of $\pi^0\gamma$ from 930,000 hadronic Z events collected in 1991 and 1992 is shown in Fig. 3. We obtain $1.12 \pm 0.22(\text{stat})$ ω mesons per hadronic Z decay, which is in a good agreement with the result obtained with the decay channel $\omega \rightarrow \pi^+\pi^-\pi^0$. The channel

Decay channel	x_p Range	JETSET		HERWIG		Production rate Measured
		Meas.	Pred.	Meas.	Pred.	
$\omega \rightarrow \pi^+\pi^-\pi^0$	$0.02 < x_p < 0.30$	0.92	1.07	0.95	0.66	$0.94 \pm 0.07 \pm 0.12$
	$0 < x_p < 1$	1.15	1.33	1.20	0.83	$1.17 \pm 0.09 \pm 0.15$
$\eta' \rightarrow \pi^+\pi^-\eta$	$0.02 < x_p < 0.30$	0.20	0.54	0.23	0.20	$0.21 \pm 0.02 \pm 0.04$
	$0 < x_p < 1$	0.25	0.67	0.28	0.25	$0.27 \pm 0.03 \pm 0.05$
$\eta' \rightarrow \rho^0\gamma$	$0.01 < x_p < 0.24$	0.20	0.54	0.19	0.20	$0.20 \pm 0.02 \pm 0.04$
	$0 < x_p < 1$	0.25	0.67	0.24	0.25	$0.24 \pm 0.02 \pm 0.05$

Table 1: Measured production rate of ω and η' mesons per hadronic Z decay. The measured values, obtained with JETSET and HERWIG Monte Carlo programs for the efficiency calculation, are reported separately. The average of the two is listed in the last column as the final result. The first error is statistical and the second systematic.

Source of systematic error	on ω rate	on η' rate	on η' rate
	$\omega \rightarrow \pi^+\pi^-\pi^0$	$\eta' \rightarrow \pi^+\pi^-\eta$	$\eta' \rightarrow \rho^0\gamma$
Selection	0.09	0.03	0.04
Detector efficiencies	0.07	0.02	0.01
Fitting	0.05	0.02	0.02
Background subtraction	0.05	0.02	0.02
Monte Carlo models	0.03	0.02	0.01
Monte Carlo statistics	0.07	0.02	0.02
Total	0.15	0.05	0.05

Table 2: Contributions to the systematic errors of the measured ω and η' production rates, added to the total in quadrature.

$\omega \rightarrow \pi^0\gamma$ is not used for the final result. Within errors, the prediction of JETSET for the ω rate is consistent with our measured rate, while the rate predicted by HERWIG is too low.

In hadronic Z decays, the vector mesons ω and ρ^0 are expected to be predominantly produced by fragmentation. Since these two mesons have the same quark content, the same spin and nearly equal mass, and thus differ only by their isospin, their production rate is expected to be equal. Using our measured production rate of ω mesons and the ALEPH and DELPHI results for ρ^0 [3,19], $N(\rho^0) = 1.29 \pm 0.12$, the ratio $N(\omega)/N(\rho^0)$ is determined to be 0.91 ± 0.16 . This result is in good agreement with the ARGUS measurement [5] of $N(\omega)/N(\rho^0) = 0.91 \pm 0.20$ and data from pp interactions [20] of $N(\omega)/N(\rho^0) = 1.02 \pm 0.08$.

Averaging the results obtained from the two η' decay channels and taking into account the common systematic errors (uncertainties in detector efficiencies and Monte Carlo models), the production rate of the η' is determined to be

$$N_{\eta'} = 0.25 \pm 0.04,$$

which is consistent with the prediction of HERWIG, but much lower than 0.67, the value predicted by JETSET 7.3.

Using our previously measured production rate of the η [21] of $0.91 \pm 0.02 \pm 0.11$, the η' to η ratio is determined to be 0.27 ± 0.06 , which is significantly lower than the value of 0.55

x_p	x_{lw}	$1/\sigma_h \cdot d\sigma/dx_p$	ξ_p	ξ_{lw}	$1/\sigma_h \cdot d\sigma/d\xi_p$
0.02–0.04	0.030	11.7 ± 2.5	3.91–3.22	3.57	0.34 ± 0.07
0.04–0.06	0.049	8.8 ± 1.8	3.22–2.81	3.02	0.43 ± 0.09
0.06–0.08	0.069	5.8 ± 1.3	2.81–2.53	2.65	0.40 ± 0.09
0.08–0.12	0.098	3.53 ± 0.82	2.53–2.12	2.28	0.35 ± 0.08
0.12–0.18	0.146	2.10 ± 0.78	2.12–1.72	1.90	0.31 ± 0.12
0.18–0.24	0.206	1.60 ± 0.52	1.72–1.43	1.56	0.33 ± 0.11
0.24–0.30	0.268	0.84 ± 0.42	1.43–1.20	1.30	0.23 ± 0.11

Table 3: Differential cross section for inclusive ω production from $\omega \rightarrow \pi^+\pi^-\pi^0$.

x_p	x_{lw}	$1/\sigma_h \cdot d\sigma/dx_p$	ξ_p	ξ_{lw}	$1/\sigma_h \cdot d\sigma/d\xi_p$
0.02–0.04	0.031	2.69 ± 0.80	3.91–3.22	3.54	0.078 ± 0.023
0.04–0.06	0.050	1.82 ± 0.54	3.22–2.81	2.99	0.090 ± 0.027
0.06–0.08	0.070	1.31 ± 0.43	2.81–2.53	2.67	0.092 ± 0.030
0.08–0.12	0.097	1.07 ± 0.34	2.53–2.12	2.36	0.105 ± 0.033
0.12–0.18	0.145	0.60 ± 0.19	2.12–1.72	1.88	0.089 ± 0.028
0.18–0.24	0.208	0.39 ± 0.14	1.72–1.43	1.55	0.080 ± 0.029

Table 4: Differential cross section for inclusive η' production from $\eta' \rightarrow \pi^+\pi^-\eta$.

from JETSET 7.3. In JETSET, the η and η' are described with the same strangeness content, which is the case if the value of the η - η' mixing angle θ_P is close to -10° . According to this description, in the string fragmentation model, the η and η' would be produced essentially with the same rate from fragmentation. Several measurements [18, 22], however, indicate a value of θ_P around -20° , which assigns more strangeness to η' and less to η . Applying the strangeness suppression factor used in JETSET to the η and η' production according to their strangeness content, the ratio η'/η from JETSET would be reduced by a factor of about 1.5, to 0.37, which is closer to our measured value. The ratio η'/η could be also reduced by the production of mesons with orbital excitation, which favor strongly the η over the η' decay modes [18]. Such mesons are not included in JETSET 7.3, but might be produced with non-negligible production rates.

Differential Cross Sections

To determine the x_p distribution, the above measurement of the production rate is repeated for different x_p intervals. Since the two Monte Carlo generators give similar efficiencies for both ω and η' mesons, we only use the high statistics JETSET Monte Carlo sample to measure the differential cross sections.

The normalized ω rate obtained in each x_p interval is listed in Table 3, where the scaled momentum value, x_{lw} , is the appropriate position [23] within the x_p bin used to plot the differential cross section. JETSET is used to calculate the value of x_{lw} (the result from HERWIG is essentially the same). In the same way we measure the momentum spectrum of η' mesons and the results are listed in Table 4 and Table 5. The x_p spectrum for ω and η' mesons is shown in Fig. 4a and Fig. 4b, respectively, together with the predictions of both models. Within errors,

x_p	x_{lw}	$1/\sigma_h \cdot d\sigma/dx_p$	ξ_p	ξ_{lw}	$1/\sigma_h \cdot d\sigma/d\xi_p$
0.01–0.04	0.028	2.32 ± 0.67	4.61–3.22	3.59	0.050 ± 0.014
0.04–0.08	0.057	1.56 ± 0.48	3.22–2.53	2.86	0.090 ± 0.028
0.08–0.12	0.097	0.89 ± 0.29	2.53–2.12	2.36	0.087 ± 0.028
0.12–0.16	0.138	0.72 ± 0.30	2.12–1.83	1.96	0.099 ± 0.041
0.16–0.24	0.198	0.40 ± 0.12	1.83–1.43	1.60	0.080 ± 0.024

Table 5: Differential cross section for inclusive η' production from $\eta' \rightarrow \rho^0 \gamma$.

x_{lw}	0.030	0.059	0.097	0.142	0.203
$1/\sigma_h \cdot d\sigma/dx_p$	2.47 ± 0.57	1.53 ± 0.30	0.96 ± 0.23	0.63 ± 0.18	0.40 ± 0.10
ξ_{lw}	3.57	2.84	2.36	1.92	1.58
$1/\sigma_h \cdot d\sigma/d\xi_p$	0.058 ± 0.013	0.091 ± 0.018	0.095 ± 0.023	0.092 ± 0.025	0.080 ± 0.020

Table 6: Differential cross section for inclusive η' production, obtained by combining the results from $\eta' \rightarrow \pi^+ \pi^- \eta$ and $\eta' \rightarrow \rho^0 \gamma$.

the shape of the measured ω and η' spectra is consistent with the prediction of both models.

For comparison with analytical calculations performed in the framework of the modified leading log approximation (MLLA) of QCD, we use the variable $\xi_p = \ln(1/x_p)$. The ξ_p values and the corresponding measured normalized rates are listed in Table 3, Table 4 and Table 5. The value ξ_{lw} referred to in the tables is calculated in the same way as the value x_{lw} . The combined results from the two η' decay channels are listed in Table 6. The measured distributions for ω and η' are shown in Fig. 5a and Fig. 5b, respectively, where for the η' the combined results from the two η' decay channels are shown. Following the same method used in our previous publications [21, 24], we fit the measured ξ_p spectra with the MLLA expression for the *limiting spectrum*:

$$\frac{1}{\sigma_{had}} \frac{d\sigma}{d\xi_p} = N(\sqrt{s}) \cdot f(\sqrt{s}, \Lambda_{eff}; \xi_p), \quad (1)$$

where σ_{had} is the total hadronic cross section, and the function f is specified in Ref. [10]. Equation (1) contains only two free parameters: an overall normalization factor N (which describes the hadronization and depends on the center of mass energy \sqrt{s} and on the particle type) and an effective scale parameter Λ_{eff} . Equation (1) is valid in the range $1 < \xi_p < \ln(0.5 \sqrt{s}/\Lambda_{eff})$. The fit results are given in Table 7, where the errors of the parameters include also the uncertainty due to a variation of the range of data points included in the fit.

Summary and Conclusions

We have studied the production of ω and η' from hadronic Z decays. The production rate of the ω is determined to be 1.17 ± 0.17 , in agreement with the JETSET prediction, but higher than the HERWIG prediction. The measured production rate of the η' and the ratio of production rates η'/η are measured to be 0.25 ± 0.04 and 0.27 ± 0.06 respectively, significantly lower than the predictions of JETSET 7.3. The low value of the ratio η'/η could be explained partially by the description of the η and η' quark content used in JETSET. The prediction of HERWIG

Meson	N	Λ_{eff} (GeV)	ξ_p^*
ω	0.127 ± 0.019	0.88 ± 0.24	2.86 ± 0.20
η'	0.033 ± 0.005	1.14 ± 0.16	2.69 ± 0.10

Table 7: Measured parameters of QCD MLLA corresponding to Equation (1). ξ_p^* denotes the position of the maximum corresponding to the given value of Λ_{eff} .

for the production rate of the η' is consistent with the measurement. The measured ω and η' production rates are consistent with the ALEPH results [3, 4].

The shape of the inclusive momentum spectrum of ω and η' is in agreement with the predictions of both Monte Carlo models. The differential cross sections as a function of ξ_p can be described by analytical QCD calculations.

Acknowledgments

We wish to express our gratitude to the CERN accelerator divisions for the excellent performance of the LEP machine. We acknowledge the contributions of all the engineers and technicians who have participated in the construction and maintenance of this experiment. Those of us who are not from member states thank CERN for its hospitality and help.

References

- [1] For a review see e.g. W. Hofmann, *Ann. ReV. Nucl. Part. Sci.* **38** (1988) 279.
- [2] For a review see e.g. A. De Angelis, “Light Quark Hadrons in Hadronic Z Decays”, CERN-PPE/95-135 and references therein.
- [3] ALEPH Collab., D. Buskulic *et al.*, *Z. Phys.* **C 69** (1996) 379.
- [4] ALEPH Collab., D. Buskulic *et al.*, *Phys. Lett.* **B 292** (1992) 210.
- [5] ARGUS Collab., H. Albrecht *et al.*, *Z. Phys.* **C 61** (1994) 1;
ARGUS Collab., H. Albrecht *et al.*, *Z. Phys.* **C 58** (1993) 199.
- [6] Mark II Collab., G. Wormser *et al.*, *Phys. Rev. Lett.* **61** (1988) 1057.
- [7] OPAL Collab., P.D. Acton *et al.*, *Phys. Lett.* **B 267** (1991) 143;
ALEPH Collab., D. Decamp *et al.*, *Z. Phys.* **C 54** (1992) 75;
DELPHI Collab., P. Abreu *et al.*, *Z. Phys.* **C 63** (1994) 17.
- [8] JETSET Monte Carlo Program:
T. Sjöstrand, *Comp. Phys. Comm.* **39** (1986) 347;
T. Sjöstrand and M. Bengtsson, *Comp. Phys. Comm.* **43** (1987) 367.
- [9] HERWIG Monte Carlo Program:
G. Marchesini and B. Webber, *Nucl. Phys.* **B 310** (1988) 461;
I.G. Knowles, *Nucl. Phys.* **B 310** (1988) 571;
G. Marchesini *et al.*, *Comp. Phys. Comm.* **67** (1992) 465.
- [10] Y.L. Dokshitzer and S.I. Troyan, Leningrad Preprint LNPI-922 (1984);
Y.I. Azimov *et al.*, *Z. Phys.* **C 27** (1985) 65;
Y.I. Azimov *et al.*, *Z. Phys.* **C 31** (1986) 213;
V.A. Khoze, Y.L. Dokshitzer and S.I. Troyan, Lund Preprint LU TP 90-12.
- [11] D. Amati and G. Veneziano, *Phys. Lett.* **B 83** (1979) 87.
- [12] L3 Collab., B. Adeva *et al.*, *Nucl. Instr. Meth.* **A 289** (1990) 35;
L3 Collab., O. Adriani *et al.*, *Phys. Rep.* **236** (1993) 1.
- [13] L3 Collab., M. Acciarri *et al.*, *Nucl. Instr. Meth.* **A 351** (1994) 300.
- [14] L3 Collab., M. Acciarri *et al.*, *Z. Phys.* **C 62** (1994) 551.
- [15] L3 Collab., B. Adeva *et al.*, *Z. Phys.* **C 55** (1992) 39.
The parameters of HERWIG have been retuned using the data of heavy flavor decays. The optimum parameters are: CLMAX=3.2, QCDLAM=0.17, VPCUT=0.5, CLPOW=1.45, B1LIM=0.35.
- [16] The L3 detector simulation is based on GEANT Version 3.14, November 1990; see R. Brun *et al.*, “GEANT 3”, CERN Preprint DD/EE/84-1 (Revised), Sept. 1987.
The GHEISHA program (H. Fesefeldt, RWTH Aachen Report PITHA 85/02 (1985)) is used to simulate hadronic interactions.

- [17] Y.J. Pei, Proc. of the “Fourth International Workshop on Software Engineering and Artificial Intelligence for High Energy and Nuclear Physics”, Pisa, 1995, eds. B. Denby and D. Perret-Gallix, World Scientific, Singapore (1995) 703.
- [18] Particle Data Group, R.M. Barnett *et al.*, Phys. Rev. **D 54** (1996) 1-I.
- [19] DELPHI Collab., P. Abreu *et al.*, Z. Phys. **C 65** (1995) 587.
- [20] M. Aguilar-Benitez *et al.* (LEBC-EHS), Z. Phys. **C 50** (1991) 405.
- [21] L3 Collab., M. Acciarri *et al.*, Phys. Lett. **B 328** (1994) 223.
- [22] F. Gilman and R. Kauffman, Phys. Rev. **D 36** (1987) 2761;
The Crystal Barrel Collab., C. Amsler *et al.*, Phys. Lett. **B 294** (1992) 451.
- [23] G.D. Lafferty and T.R. Wyatt, Nucl. Instr. and Meth. **A 355** (1995) 541.
- [24] L3 Collab., B. Adeva *et al.*, Phys. Lett. **B 259** (1991) 199;
L3 Collab., O. Adriani *et al.*, Phys. Lett. **B 286** (1992) 403.

The L3 Collaboration:

M. Acciarri,²⁸ O. Adriani,¹⁷ M. Aguilar-Benitez,²⁷ S. Ahlen,¹¹ B. Alpat,³⁵ J. Alcaraz,²⁷ G. Alemanni,²³ J. Allaby,¹⁸ A. Aloisio,³⁰ G. Alverson,¹² M. G. Alvigi,³⁰ G. Ambrosi,²⁰ H. Anderhub,⁵⁰ V. P. Andreev,³⁹ T. Angelescu,¹³ F. Anselmo,⁹ D. Antreasyan,⁹ A. Arefiev,²⁹ T. Azemoon,³ T. Aziz,¹⁰ P. Bagnaia,³⁸ L. Baksay,⁴⁵ R. C. Ball,³ S. Banerjee,¹⁰ K. Banicz,⁴⁷ R. Barillère,¹⁸ L. Barone,³⁸ P. Bartalini,³⁵ A. Baschirotto,²⁸ M. Basile,⁹ R. Battiston,³⁵ A. Bay,²³ F. Becattini,¹⁷ U. Becker,¹⁶ F. Behner,⁵⁰ J. Berdugo,²⁷ P. Berges,¹⁶ B. Bertucci,¹⁸ B. L. Betev,⁵⁰ S. Bhattacharya,¹⁰ M. Biasini,¹⁸ A. Biland,⁵⁰ G. M. Bilei,³⁵ J. J. Blaising,¹⁸ S. C. Blyth,³⁶ G. J. Bobbink,² R. Bock,¹ A. Böhm,¹ B. Borgia,³⁸ A. Boucham,⁴ D. Bourilkov,⁵⁰ M. Bourquin,²⁰ D. Boutigny,⁴ J. G. Branson,⁴¹ V. Brigljevic,⁵⁰ I. C. Brock,³⁶ A. Buffini,¹⁷ A. Buijs,⁴⁶ J. D. Burger,¹⁶ W. J. Burger,²⁰ J. Busenitz,⁴⁵ A. Buytenhuijs,³² X. D. Cai,¹⁶ M. Campanelli,⁵⁰ M. Capell,¹⁶ G. Cara Romeo,⁹ M. Caria,³⁵ G. Carlino,⁴ A. M. Cartacci,¹⁷ J. Casaus,²⁷ G. Castellini,¹⁷ F. Cavallari,³⁸ N. Cavallo,³⁰ C. Cecchi,²⁰ M. Cerrada,²⁷ F. Cesaroni,²⁴ M. Chamizo,²⁷ A. Chan,⁵² Y. H. Chang,⁵² U. K. Chaturvedi,¹⁹ M. Chemarin,²⁶ A. Chen,⁵² G. Chen,⁷ G. M. Chen,⁷ H. F. Chen,²¹ H. S. Chen,⁷ M. Chen,¹⁶ G. Chiefari,³⁰ C. Y. Chien,⁵ M. T. Choi,⁴⁴ L. Cifarelli,⁴⁰ F. Cindolo,⁹ C. Civinini,¹⁷ I. Clare,¹⁶ R. Clare,¹⁶ H. O. Cohn,³³ G. Coignet,⁴ A. P. Colijn,² N. Colino,²⁷ V. Commichau,³ S. Costantini,³⁸ F. Cotorobai,¹³ B. de la Cruz,²⁷ A. Csilling,¹⁴ T. S. Dai,¹⁶ R. D'Alessandro,¹⁷ R. de Asmundis,³⁰ H. De Boeck,³² A. Degré,⁴ K. Deiters,⁴⁸ P. Denes,³⁷ F. DeNotaristefani,³⁸ D. DiBitonto,⁴⁵ M. Diemoz,³⁸ D. van Dierendonck,² F. Di Lodovico,⁵⁰ C. Dionisi,³⁸ M. Dittmar,⁵⁰ A. Dominguez,⁴¹ A. Doria,³⁰ I. Dorne,⁴ M. T. Dova,^{19,2} E. Drago,³⁰ D. Duchesneau,⁴ P. Duinker,² I. Duran,⁴² S. Dutta,¹⁰ S. Easo,³⁵ Yu. Efremenko,³³ H. El Mamouni,²⁶ A. Engler,³⁶ F. J. Eppling,¹⁶ F. C. Erné,² J. P. Ernenwein,²⁶ P. Extermann,²⁰ M. Fabre,⁴⁸ R. Faccini,³⁸ S. Falciano,³⁸ A. Favara,¹⁷ J. Fay,²⁶ O. Fedin,³⁹ M. Felcini,⁵⁰ B. Fenyi,⁴⁵ T. Ferguson,³⁶ D. Fernandez,²⁷ F. Ferroni,³⁸ H. Fesefeldt,¹ E. Fiandrini,³⁵ J. H. Field,²⁰ F. Filthaut,³⁶ P. H. Fisher,¹⁶ G. Forconi,¹⁶ L. Fredj,²⁰ K. Freudenreich,⁵⁰ C. Furetta,²⁸ Yu. Galaktionov,^{29,16} S. N. Ganguli,¹⁰ P. Garcia-Abia,²⁷ S. S. Gau,¹² S. Gentile,³⁸ J. Gerald,⁵ N. Gheordanescu,¹³ S. Giagu,³⁸ S. Goldfarb,²³ J. Goldstein,¹¹ Z. F. Gong,²¹ A. Gougas,⁵ G. Gratta,³⁴ M. W. Gruenewald,³ V. K. Gupta,³⁷ A. Gurtu,¹⁰ L. J. Gutay,⁴⁷ B. Hartmann,¹ A. Hasan,³¹ D. Hatzifotiadou,⁹ T. Hebbeker,⁸ A. Hervé,¹⁸ W. C. van Hoek,³² H. Hofer,⁵⁰ H. Hoorani,²⁰ S. R. Hou,⁵² G. Hu,⁵ V. Innocenti,¹⁸ H. Janssen,⁴ K. Jenkes,¹ B. N. Jin,⁷ L. W. Jones,³ P. de Jong,¹⁸ I. Josa-Mutuberria,²⁷ A. Kasser,²³ R. A. Khan,¹⁹ D. Kamrad,⁴⁹ Yu. Kamyshev,³³ J. S. Kapustinsky,²⁵ Y. Karyotakis,⁴ M. Kaur,^{19,4} M. N. Kienzle-Focacci,²⁰ D. Kim,⁵ J. K. Kim,⁴⁴ S. C. Kim,⁴⁴ Y. G. Kim,⁴⁴ W. W. Kinnison,²⁵ A. Kirkby,³⁴ D. Kirkby,³⁴ J. Kirkby,¹⁸ D. Kiss,¹⁴ W. Kittel,³² A. Klimentov,^{16,29} A. C. König,³² I. Korolko,²⁹ V. Koutsenko,^{16,29} R. W. Kraemer,³⁶ W. Krenz,¹ H. Kuijten,³² A. Kunin,^{16,29} P. Ladron de Guevara,²⁷ G. Landi,¹⁷ C. Lapoint,¹⁶ K. Lassila-Perini,⁵⁰ P. Laurikainen,²² M. Lebeau,¹⁸ A. Lebedev,¹⁶ P. Lebrun,²⁶ P. Lecomte,⁵⁰ P. Lecoq,¹⁸ P. Le Coultre,⁵⁰ J. S. Lee,⁴⁴ K. Y. Lee,⁴⁴ C. Leggett,³ J. M. Le Goff,¹⁸ R. Leiste,⁴⁹ E. Leonardi,³⁸ P. Levchenko,³ C. Li,²¹ E. Lieb,⁴⁹ W. T. Lin,⁵² F. L. Linde,^{2,18} L. Lista,³⁰ Z. A. Liu,⁷ W. Lohmann,⁴⁹ E. Longo,³⁸ W. Lu,³⁴ Y. S. Lu,⁷ K. Lübelmeyer,¹ C. Luci,³⁸ D. Luckey,¹⁶ L. Luminari,³⁸ W. Lustermaun,⁴⁸ W. G. Ma,²¹ M. Maity,¹⁰ G. Majumder,¹⁰ L. Malgeri,¹ A. Malinin,²⁹ C. Mañá,²⁷ S. Mangla,¹⁰ P. Marchesini,⁵⁰ A. Marin,¹¹ J. P. Martin,²⁶ F. Marzano,³⁸ G. G. G. Massaro,² D. McNally,¹⁸ S. Mele,³⁰ L. Merola,³⁰ M. Meschini,⁷ W. J. Metzger,³² M. von der Mey,¹ Y. Mi,²³ A. Mihul,¹³ A. J. W. van Mil,³² G. Mirabelli,³⁸ J. Mnich,¹⁸ P. Molnar,⁸ B. Monteleoni,¹⁷ R. Moore,³ S. Morganti,³⁸ T. Moulík,¹⁰ R. Mount,³⁴ S. Müller,¹ F. Muheim,²⁰ E. Nagy,¹⁴ S. Nahn,¹⁶ M. Napolitano,³⁰ F. Nessi-Tedaldi,⁵⁰ H. Newman,³⁴ T. Niessen,¹ A. Nippe,¹ A. Nisati,³⁸ H. Nowak,⁴⁹ H. Opitz,¹ G. Organtini,³⁸ R. Ostonen,²² D. Pandoulas,¹ S. Paoletti,³⁸ P. Paolucci,³⁰ H. K. Park,³⁶ G. Pascale,³⁸ G. Passaleva,¹⁷ S. Patricelli,³⁰ T. Paul,¹² M. Pauluzzi,³⁵ C. Paus,¹ F. Pauss,⁵⁰ D. Peach,¹⁸ Y. J. Pei,¹ S. Pensotti,²⁸ D. Perret-Gallix,⁴ S. Petrak,⁸ A. Pevsner,⁵ D. Piccolo,³⁰ M. Pieri,¹⁷ J. C. Pinto,³⁶ P. A. Piroué,³⁷ E. Pistolesi,²⁸ V. Plyaskin,²⁹ M. Pohl,⁵⁰ V. Pojidaev,^{29,17} H. Postema,¹⁶ N. Produit,²⁰ D. Prokofiev,³⁹ G. Rahal-Callot,⁵⁰ P. G. Rancoita,²⁸ M. Rattaggi,²⁸ G. Raven,⁴¹ P. Razis,³¹ K. Read,³³ D. Ren,⁵⁰ M. Rescigno,³⁸ S. Reucroft,¹² T. van Rhee,⁴ S. Riemann,⁴⁹ B. C. Riemers,⁴⁷ K. Riles,³ O. Rind,³ S. Ro,⁴⁴ A. Robohn,⁵⁰ J. Rodin,¹⁶ F. J. Rodriguez,²⁷ B. P. Roe,³ L. Romero,²⁷ S. Rosier-Lees,⁴ Ph. Rosselet,²³ W. van Rossum,⁴⁶ S. Roth,¹ J. A. Rubio,¹⁸ H. Rykaczewski,⁵⁰ J. Salicio,¹⁸ E. Sanchez,²⁷ A. Santocchia,³⁵ M. E. Sarakinos,²² S. Sarkar,¹⁰ M. Sassowsky,¹ G. Sauvage,⁴ C. Schäfer,¹ V. Schegelsky,³⁹ S. Schmidt-Kaerst,¹ D. Schmitz,¹ P. Schmitz,¹ M. Schneegans,⁴ N. Scholz,⁵⁰ H. Schopper,⁵¹ D. J. Schotanus,³² J. Schwenke,¹ G. Schwering,¹ C. Sciacca,³⁰ D. Sciarrino,²⁰ J. C. Sens,⁵² L. Servoli,³⁵ S. Shevchenko,³⁴ N. Shivarov,⁴³ V. Shoutko,²⁹ J. Shukla,²⁵ E. Shumilov,²⁹ A. Shvorob,³⁴ T. Siedenburt,¹ D. Son,⁴⁴ A. Sopczak,⁴⁹ V. Soulimov,³⁰ B. Smith,¹⁶ P. Spillantini,¹⁷ M. Steuer,¹⁶ D. P. Stickland,³⁷ H. Stone,³⁷ B. Stoyanov,⁴³ A. Straessner,¹ K. Strauch,¹⁵ K. Sudhakar,¹⁰ G. Sultanov,¹⁹ L. Z. Sun,²¹ G. F. Susinno,²⁰ H. Suter,⁵⁰ J. D. Swain,¹⁹ X. W. Tang,⁷ L. Tauscher,⁶ L. Taylor,¹² Samuel C. C. Ting,¹⁶ S. M. Ting,¹⁶ M. Tonutti,¹ S. C. Tonwar,¹⁰ J. Tóth,¹⁴ C. Tully,³⁷ H. Tuchscherer,⁴⁵ K. L. Tung,⁷ Y. Uchida,¹⁶ J. Ulbricht,⁵⁰ U. Uwer,¹⁸ E. Valente,³⁸ R. T. Van de Walle,³² G. Vesztegombi,¹⁴ I. Vetlitsky,²⁹ G. Viertel,⁵⁰ M. Vivargent,⁴ R. Völkert,⁴⁹ H. Vogel,³⁶ H. Vogt,⁴⁹ I. Vorobiev,²⁹ A. A. Vorobyov,³⁹ A. Vorvolakos,³¹ M. Wadhwa,⁵ W. Wallraff,¹ J. C. Wang,¹⁶ X. L. Wang,²¹ Z. M. Wang,²¹ A. Weber,¹ F. Wittgenstein,¹⁸ S. X. Wu,¹⁹ S. Wynhoff,¹ J. Xu,¹¹ Z. Z. Xu,²¹ B. Z. Yang,²¹ C. G. Yang,⁷ X. Y. Yao,⁷ J. B. Ye,²¹ S. C. Yeh,⁵² J. M. You,³⁶ An. Zalite,³⁹ Yu. Zalite,³⁹ P. Zemp,⁵⁰ Y. Zeng,¹ Z. Zhang,⁷ Z. P. Zhang,²¹ B. Zhou,¹¹ Y. Zhou,³ G. Y. Zhu,⁷ R. Y. Zhu,³⁴ A. Zichichi,^{9,18,19} F. Ziegler.⁴⁹

- 1 I. Physikalisches Institut, RWTH, D-52056 Aachen, FRG[§]
 - III. Physikalisches Institut, RWTH, D-52056 Aachen, FRG[§]
 - 2 National Institute for High Energy Physics, NIKHEF, and University of Amsterdam, NL-1009 DB Amsterdam, The Netherlands
 - 3 University of Michigan, Ann Arbor, MI 48109, USA
 - 4 Laboratoire d'Annecy-le-Vieux de Physique des Particules, LAPP, IN2P3-CNRS, BP 110, F-74941 Annecy-le-Vieux CEDEX, France
 - 5 Johns Hopkins University, Baltimore, MD 21218, USA
 - 6 Institute of Physics, University of Basel, CH-4056 Basel, Switzerland
 - 7 Institute of High Energy Physics, IHEP, 100039 Beijing, China[△]
 - 8 Humboldt University, D-10099 Berlin, FRG[§]
 - 9 INFN-Sezione di Bologna, I-40126 Bologna, Italy
 - 10 Tata Institute of Fundamental Research, Bombay 400 005, India
 - 11 Boston University, Boston, MA 02215, USA
 - 12 Northeastern University, Boston, MA 02115, USA
 - 13 Institute of Atomic Physics and University of Bucharest, R-76900 Bucharest, Romania
 - 14 Central Research Institute for Physics of the Hungarian Academy of Sciences, H-1525 Budapest 114, Hungary[‡]
 - 15 Harvard University, Cambridge, MA 02139, USA
 - 16 Massachusetts Institute of Technology, Cambridge, MA 02139, USA
 - 17 INFN Sezione di Firenze and University of Florence, I-50125 Florence, Italy
 - 18 European Laboratory for Particle Physics, CERN, CH-1211 Geneva 23, Switzerland
 - 19 World Laboratory, FBLJA Project, CH-1211 Geneva 23, Switzerland
 - 20 University of Geneva, CH-1211 Geneva 4, Switzerland
 - 21 Chinese University of Science and Technology, USTC, Hefei, Anhui 230 029, China[△]
 - 22 SEFT, Research Institute for High Energy Physics, P.O. Box 9, SF-00014 Helsinki, Finland
 - 23 University of Lausanne, CH-1015 Lausanne, Switzerland
 - 24 INFN-Sezione di Lecce and Università Degli Studi di Lecce, I-73100 Lecce, Italy
 - 25 Los Alamos National Laboratory, Los Alamos, NM 87544, USA
 - 26 Institut de Physique Nucléaire de Lyon, IN2P3-CNRS, Université Claude Bernard, F-69622 Villeurbanne, France
 - 27 Centro de Investigaciones Energeticas, Medioambientales y Tecnologicas, CIEMAT, E-28040 Madrid, Spain^b
 - 28 INFN-Sezione di Milano, I-20133 Milan, Italy
 - 29 Institute of Theoretical and Experimental Physics, ITEP, Moscow, Russia
 - 30 INFN-Sezione di Napoli and University of Naples, I-80125 Naples, Italy
 - 31 Department of Natural Sciences, University of Cyprus, Nicosia, Cyprus
 - 32 University of Nymegen and NIKHEF, NL-6525 ED Nymegen, The Netherlands
 - 33 Oak Ridge National Laboratory, Oak Ridge, TN 37831, USA
 - 34 California Institute of Technology, Pasadena, CA 91125, USA
 - 35 INFN-Sezione di Perugia and Università Degli Studi di Perugia, I-06100 Perugia, Italy
 - 36 Carnegie Mellon University, Pittsburgh, PA 15213, USA
 - 37 Princeton University, Princeton, NJ 08544, USA
 - 38 INFN-Sezione di Roma and University of Rome, "La Sapienza", I-00185 Rome, Italy
 - 39 Nuclear Physics Institute, St. Petersburg, Russia
 - 40 University and INFN, Salerno, I-84100 Salerno, Italy
 - 41 University of California, San Diego, CA 92093, USA
 - 42 Dept. de Fisica de Particulas Elementales, Univ. de Santiago, E-15706 Santiago de Compostela, Spain
 - 43 Bulgarian Academy of Sciences, Central Laboratory of Mechatronics and Instrumentation, BU-1113 Sofia, Bulgaria
 - 44 Center for High Energy Physics, Korea Advanced Inst. of Sciences and Technology, 305-701 Taejon, Republic of Korea
 - 45 University of Alabama, Tuscaloosa, AL 35486, USA
 - 46 Utrecht University and NIKHEF, NL-3584 CB Utrecht, The Netherlands
 - 47 Purdue University, West Lafayette, IN 47907, USA
 - 48 Paul Scherrer Institut, PSI, CH-5232 Villigen, Switzerland
 - 49 DESY-Institut für Hochenergiephysik, D-15738 Zeuthen, FRG
 - 50 Eidgenössische Technische Hochschule, ETH Zürich, CH-8093 Zürich, Switzerland
 - 51 University of Hamburg, D-22761 Hamburg, FRG
 - 52 High Energy Physics Group, Taiwan, China
- [§] Supported by the German Bundesministerium für Bildung, Wissenschaft, Forschung und Technologie
[‡] Supported by the Hungarian OTKA fund under contract number T14459.
^b Supported also by the Comisión Interministerial de Ciencia y Tecnología
[‡] Also supported by CONICET and Universidad Nacional de La Plata, CC 67, 1900 La Plata, Argentina
[◇] Also supported by Panjab University, Chandigarh-160014, India
[△] Supported by the National Natural Science Foundation of China.

Figure Captions

- Figure 1 The measured $\pi^+\pi^-\pi^0$ invariant mass distribution. The solid line represents the result of the fit to the data using a sum of a Gaussian distribution and a background shape as described in the text. The dashed line indicates the fitted background.
- Figure 2 The measured (a) $\pi^+\pi^-\eta$ and (b) $\rho^0\gamma$ invariant mass distributions. The solid lines represent the results of the fits to the data using a sum of a Gaussian distribution and a background shape as described in the text. The dashed lines indicate the fitted background.
- Figure 3 The measured $\pi^0\gamma$ invariant mass distribution. The solid line represents the result of the fit to the data using a sum of a Gaussian distribution and a background shape as described in the text. The dashed line indicates the fitted background.
- Figure 4 The x_p distribution of the (a) ω and (b) η' at the Z resonance normalized to the total hadronic cross section in comparison with the predictions of JETSET and HERWIG. The bin ranges are given in Table 3, 4, and 5.
- Figure 5 The ξ_p distribution of the (a) ω and (b) η' at the Z resonance normalized to the total hadronic cross section, compared with analytical QCD calculations in the range of validity of Equation (1). In Fig. 5b the results from the two η' decay channels are combined. The bin ranges are given in Table 3 and 6.

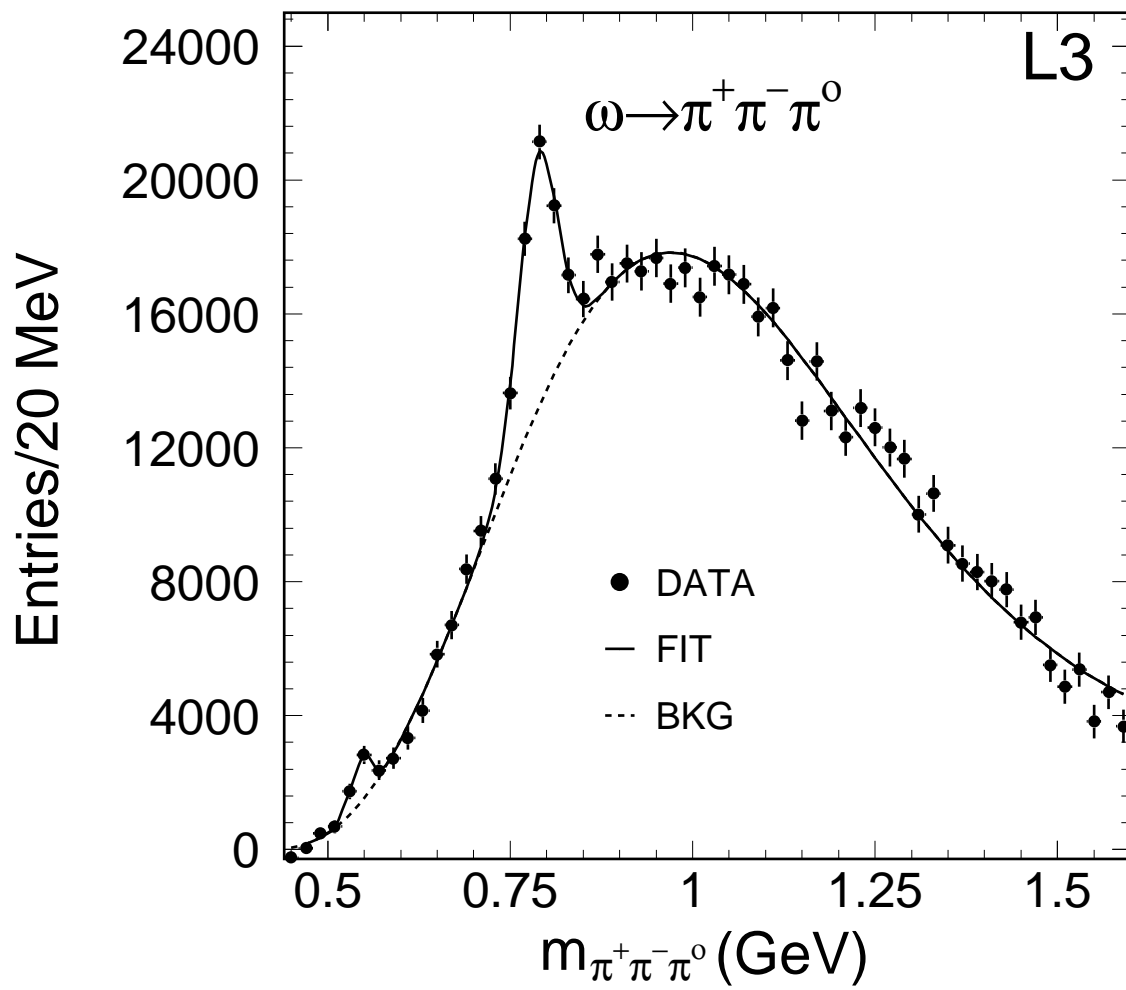


Figure 1

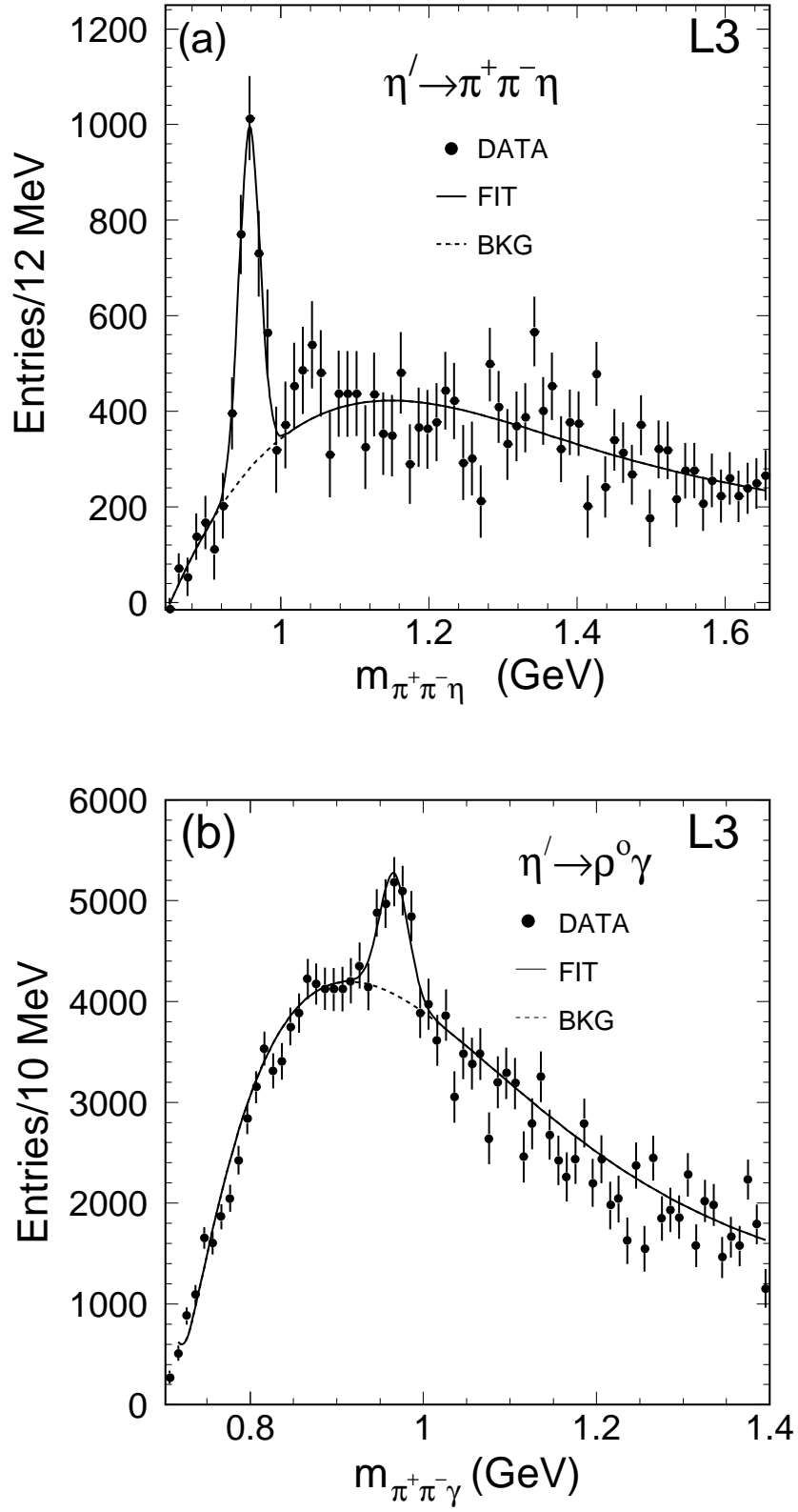


Figure 2

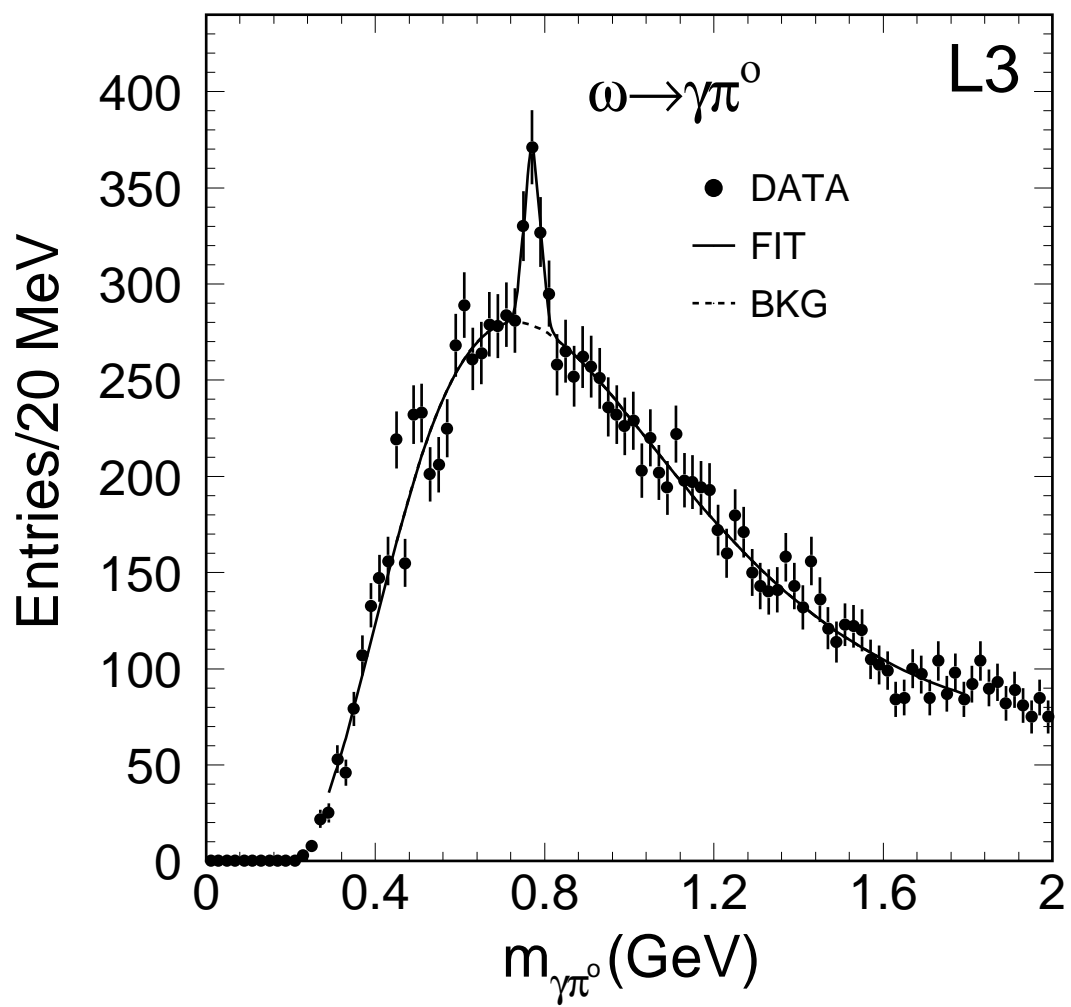


Figure 3

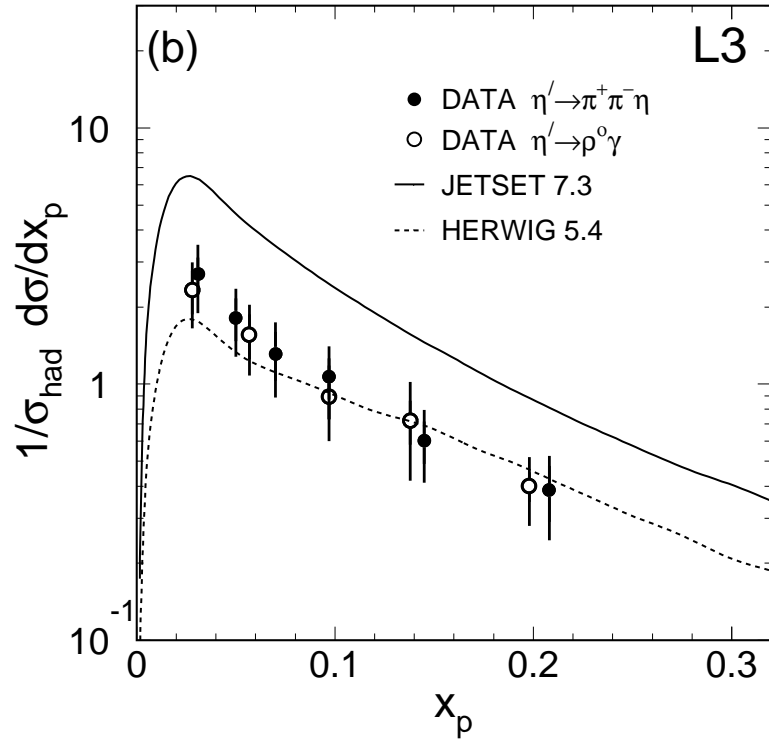
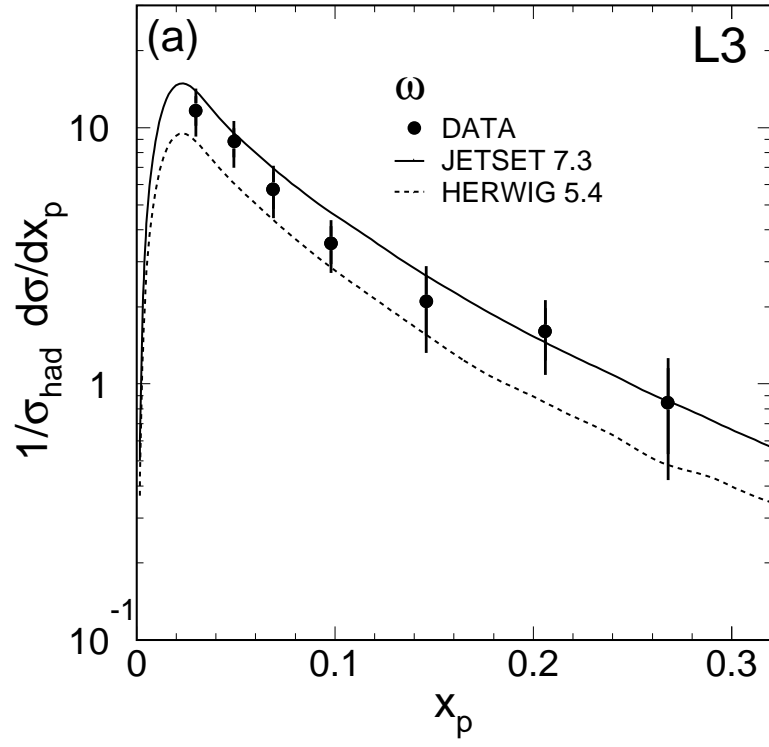


Figure 4

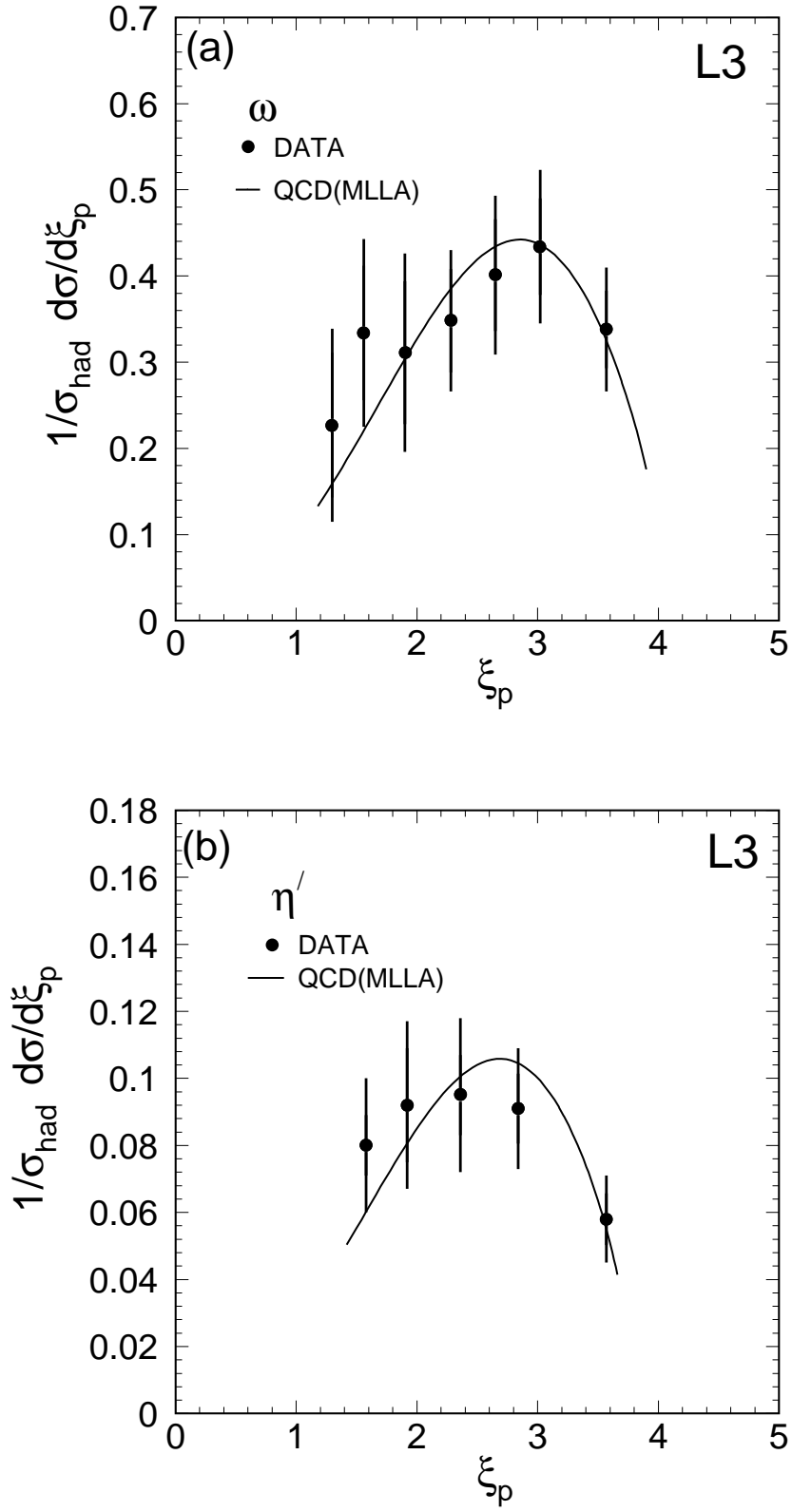


Figure 5